

Influence of the Pressure on Spatial and Temporal Resolved Plasma Physical Parameters of a TCI-Ignition System

Tobias Michler, Olaf Toedter, Thomas Koch

Abstract

In this work, the influence of pressure on the electrical parameters of a standard automotive ignition system and the characteristic spectra of the ignition spark were shown. The spectrum of the breakdown shows the strongest change, from a relatively discrete N_2 band spectrum to a bright continuum spectrum with intense NII line radiation in it. In the arc discharge, the metal lines from the electrode material dominate the shape of the spectrum. These lines can be used to determine the excitation temperature and to estimate the intensity with which the electrode material is released by the thermionic effects of the discharge. Lastly, the shape of the glow discharges is not affected by the pressure, only their intensity decreases. Because of the differences in the spectra, several methods are needed to determine different temperatures or other plasma characteristics.

1 Introduction

1.1 Motivation

The phases of the ignition spark were first described by the observations of Maly [1–8]. He divided the spark into the three phases of the breakdown, the arc and the glow discharge, which differ of their plasma-physical mechanism of electron supply. These different mechanisms resulting in different inflammation and erosion behavior of the phases, which are summarized in Fig. 1.

Influence of the Pressure on Spatial and Temporal Resolved Plasma Physical Parameters on a TCI-Ignition System

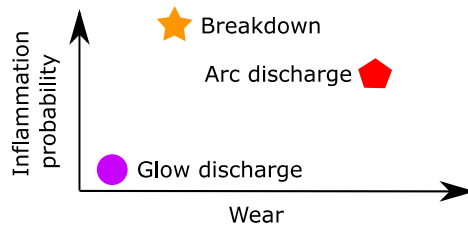


Fig. 1: Connection between the inflammation probability and the potential of electrode wear of the three ignition phases.

In addition to the phases, the knowledge of the electrical structure of an ignition system is necessary. Therefore, Fig. 2 shows as an example the schematic of an electrical circuit of a standard automotive ignition system, consisting of inductors, capacitors and resistors. The location of these resistances affects the discharge characteristics of the remaining elements by increasing or decreasing their time constants, depending on whether the element is an inductance or capacitance. A closer look to the capacitances of the system, the spark plug comes more into the focus. It can be divided into a capacitance in front of the suppressor resistance C_{SP1} and behind it C_{SP2} , resulting in different discharge behavior of these two capacitances [9]. Especially the second one is interesting, because it is not inhibiting by the resistance and can discharge extremely fast.

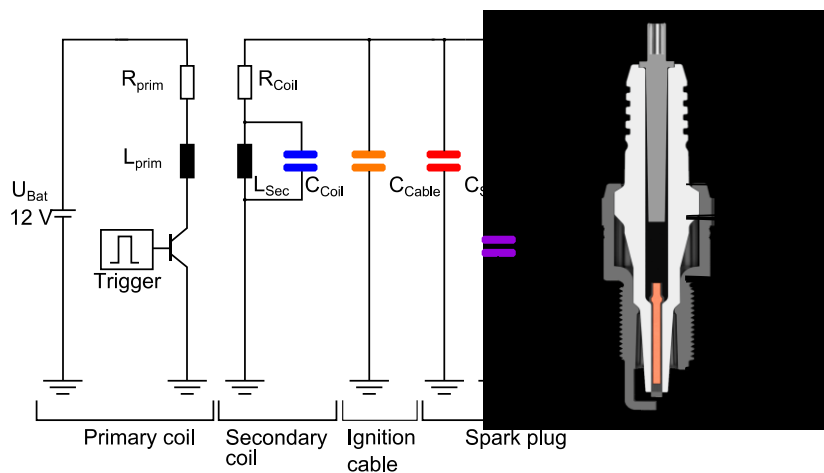


Fig. 2: Connection between the inflammation probability and the potential of electrode wear of the three ignition phases.

Influence of the Pressure on Spatial and Temporal Resolved Plasma Physical Parameters on a TCI-Ignition System

Therefore, the connection between ignition system design, the ignition phases, the erosion and inflammation behavior need further observation. In this work, a study on the influence of the pressure on the spectrum of the ignition phases is done.

1.2 Plasmaphysical Basics

In the following subsection, the plasma physical basics of the three phases are roughly outlined to illustrate some special features of the measurements.

1.2.1 Breakdown

The breakdown process begins with the avalanche or townsend mechanism described by Townsend [11–13]. It begins with a start electron supplied by radiation, field emission or similar. This electron is accelerated by the electric field and accumulates energy. If the energy is too low for ionization, the electron-particle collisions are elastic and there is no energy loss for the electrons. Once the energy exceeds the ionization energy of the electron collision partner, the particle is ionized and the colliding electron loses its energy by inelastic collisions. Afterwards, the two electrons move further in the direction of the anode and get accelerated, and the process repeats. The resulting ions move towards the cathode and release new electrons at this electrode by secondary electron emission. These electrons starting new avalanches until a conductive channel is formed. This process requires more than one avalanche to form this channel.

As soon as the electron number reaches a critical value of 10^8 [14], the space-charge cannot be neglected compared to the external field, which marks the transition to the so-called streamer mechanism described by Loeb, Meek and Raether [15–17]. The fast electrons leave the slow ions behind, forming a negatively charged streamer head and positively charged streamer tail. Increased recombination processes occur between these two regions. In addition, ionization and recombination are enhanced in front of the streamer head due to the high field strengths. This leads to radiation, which can also ionize the gas again even at a greater distance. Therefore, the streamer can move very fast forward to the anode. The time to form a conductive channel with this process is in the range of ten ns. Moreover, the streamer can form a conductive channel with only a single avalanche.

1.2.2 Arc Discharge

The arc discharge is characterized by its high current densities, which can only be delivered by thermionic-field emission [18]. In this process, the electrode material melts and evaporates in a very localized area of some tens μm in each plasma channel [19]. This area is called cathode spot. In addition, atomic oxygen produces in the plasma column form volatile metal oxides with the electrode material, transporting them into the gas [10]. There, the metal can be ionized and form a strong electric field to the cathode in which electrons can be released from the cathode by field emission. These processes are very efficient in supplying electrons and therefore require a low burning voltage of the plasma [20]. Furthermore, the metal atoms can be detected with a spectrograph and are thus a direct indicator of the arc discharge.

1.2.3 Glow Discharge

In contrast to the arc discharge, in the glow discharges electron supply happens in the gas takes place by electron collisions. The spatial structure of the glow discharge is the most complex of the three ignition phases and can be divided into three relevant areas [21, 22]. In the negative glow area, high ionization lead to high inhomogeneous electrical field strength near the cathode, which results in a high cathode fall and burning voltage of the discharge [23]. This area is by far the brightest of the glow discharge. Next is the area of the positive column, which is significantly darker. In this area, electrons are accelerated by the constant homogenous field, resulting in uniform radiation. Near the anode, electrons accumulate, flow off into it and form the region of the so-called anode glow, which is slightly brighter than the radiation of the positive column.

2 Experimental Setup and Methodology

The ignition coil used in these experiments is a commercial cassette coil system for passenger cars. It has a secondary energy of 90 mJ and an initial spark current

Influence of the Pressure on Spatial and Temporal Resolved Plasma Physical Parameters on a TCI-Ignition System

of 150 mA at atmospheric pressure. A commercial tip-to-tip j-gap spark plug with an IrRh10 alloy at the center electrode and PtRh30 at the ground electrode is used. The electrode diameters and spacing are 0.6 mm and 0.9 mm, respectively. The suppressor resistance is 4.2 k Ω and the total capacitance of the spark plug is 12 pF. Due to the geometry of the spark plug, this capacitance can be divided into the two capacitances C_{SP1} and C_{SP2} with 4 and 8 pf, respectively. Ignition coil and spark plug are connected by a high-voltage cable without resistance. The spark plug is fitted into a pressure chamber filled with synthetic air (79 vol.-% N₂ and 21 vol.-% O₂)

2.1 Spectroscopic and Electrical setup

2.1.1 Spectroscopic Setup

A scheme of the experimental electrical and spectroscopic setup used is shown in Fig. 3. The core element is the Acton SP2556 grating spectrograph from Princeton Instruments. Its focal length is 500 mm and has an adjustable inlet slit width between 10 and 3000 μm . In addition, it has three different gratings with 150, 600 and 1200 lines/mm mounted on a turret, which can be easily switched between.

Mounted on the spectrograph is a PI-MAX 2 ICCD camera from Princeton Instruments with a multichannel plate (MCP) amplifier. The chip used has a dimension of 1024x256 pixels in direction of the wavelength and axial to the spark plug gap, respectively. Therefore, an analysis of the plasma over the spark plug gap is possible. The ignition spark uses 58 pixels in the height, which results in a resolution of 16 μm /pixel. During the investigations, 20 additional pixels are evaluated because the glow of the glow discharge protrudes beyond the center electrode.

Three combinations of slit width and gratings are used in this work, resulting in different instrumental broadenings of the system. These broadenings were measured using a LOT-Oriel LSP035 mercury-argon arc lamp. For high resolution, the 1200 lines/mm grating in combination with a 10 μm slit is used. This results in an instrumental broadening of less than 0.1 nm. A medium resolution was achieved with the 600 lines/mm grating and a slit width of 200 μm , resulting in an instrumental broadening of 0.7 nm. To detect a wide range of wavelengths,

2.2 Methodology

2.2.1 Methodology of Data Collection

The gating of the camera is recorded with the oscilloscope. Therefore, the point in time of the ignition spark and the acquired spectrum can be matched with this signal. This technique allows to differentiate between the different spark phases under consideration of the measured voltage and currents. To increase the accuracy of the following post processing, 50 spectra are acquired and then averaged. The determination of the three phases had to be performed with different exposure times and gains due to their different time intervals and intensities. In the arc and glow phase of the spark, the gain was in maximum setting and the exposure time was adjusted in the range of 100 to 200 μs to sustain acceptable signal-to-noise ratios of the signals. The short duration of the breakdown resulted in short exposure times of 2 μs .

2.2.2 Determination of Electrical Energy

With the voltage curve of the ignition spark, the supplied energy to the different spark phases can be determined. Fig. 4 shows the voltage profile of 200 sparks. For clarification of the relevant voltage levels, the breakdown voltage is cut off. The two voltage levels with a difference of approximately 300 V are clearly visible. It is also noticeable that the arc discharge is not found over the entire duration of the ignition spark and is found at higher currents.

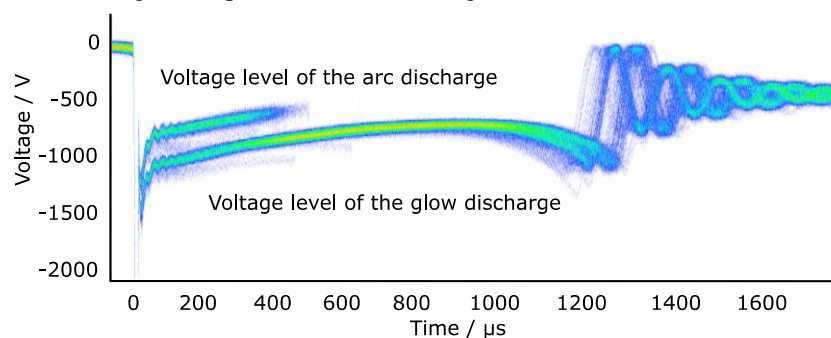


Fig. 4: Persistent plot of 200 ignition sparks at a pressure of 6 bar.

Influence of the Pressure on Spatial and Temporal Resolved Plasma Physical Parameters on a TCI-Ignition System

The calculation of the electrical energy of each phase can be done with the following two equations (1) and (2).

$$E_{BD} = \frac{1}{2} C_{SP2} * U_{BD}^2 \quad (1)$$

$$E_D = \int u_D(t) * (1 - R_{SP} * i_D(t)) * i_D(t) dt \quad (2)$$

In these equations, E is the electrical energy of the breakdown (BD) and the inductive discharge (D). The other parameters are the capacitance C_{SP2} of the spark plug, the breakdown voltage U_{BD} , the discharge current and voltage $i_D(t)$ and $u_D(t)$, and the spark plug resistance R_{SP} .

3 Results and Discussion

3.1 Pressure Influence on Electrical Parameters

First, the electrical behavior of the ignition system used must be evaluated under different pressures. Starting with the behavior of the breakdown voltage U_{BD} in the upper graph of Fig. 5. In addition, the static breakdown voltage U_{Stat} , calculated by paschen's law, and the ratio of both U_{BD}/U_{Stat} are shown here. At low pressures below five bar, the measured breakdown voltage is much higher compared to the static voltage. This is can be explained by the absence of a start electron for the avalanche process in the dark and shielded pressure chamber [26]. With increasing pressure, this start electron is more likely supplied by field emission from the electrodes [14], therefore the ratio decreases. In addition, the voltage slope of charging the secondary capacitances decreases also due to electrical behavior of the ignition coil, which gives the discharge more time to form a conductive channel.

The increase in breakdown voltage results in an increase in the energy stored by the capacitances and therefore decrease the energy stored in the inductance. As a consequence, the initial current of the inductive discharge also decreases, which is shown in the bottom left graph of Fig. 5. In the case of the ignition coil

Influence of the Pressure on Spatial and Temporal Resolved Plasma Physical Parameters on a TCI-Ignition System

used, the current decreases in two steps. Between atmospheric pressure and eight bar absolute pressure, the current is reduced from -150 to -140 mA. In the second step, this decrease is much stronger and reduces this initial current to approximately -100 mA.

Finally, these effects also influence the duration of the glow and arc discharge, which is shown in Fig. 5 (bottom right). The area between both discharges shows the duration of the respective discharge. The top line shows the total duration of the ignition spark. As the pressure increases, the spark shortens due to the lower energy in the inductance. However, an increase in the arc duration can be observed. The higher pressures support higher charge carrier densities, which can lead to arc discharges. On the other hand, the reduction of initial current can lead to the opposite effect and reduces the arcs duration slightly, which explains the maximum between six and eight bar and the subsequent reduction.

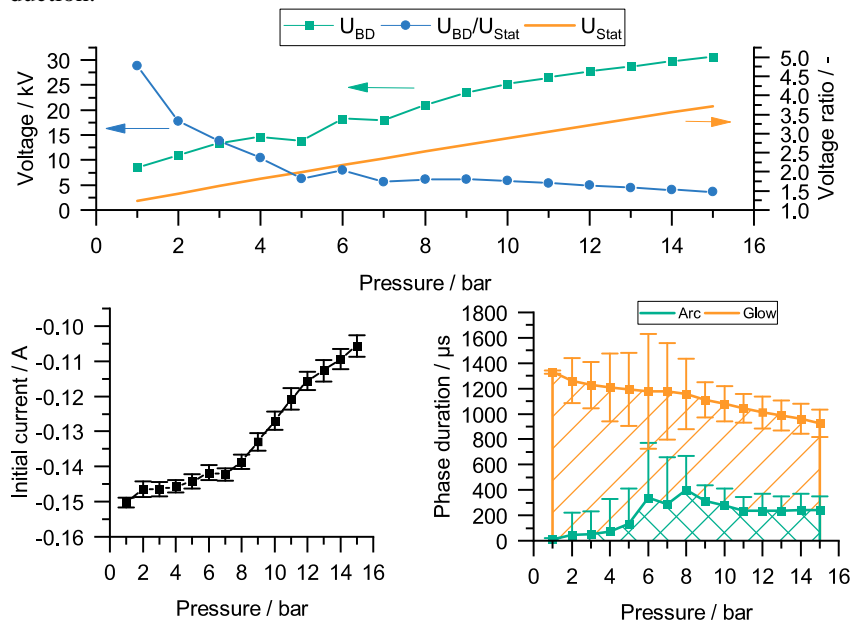
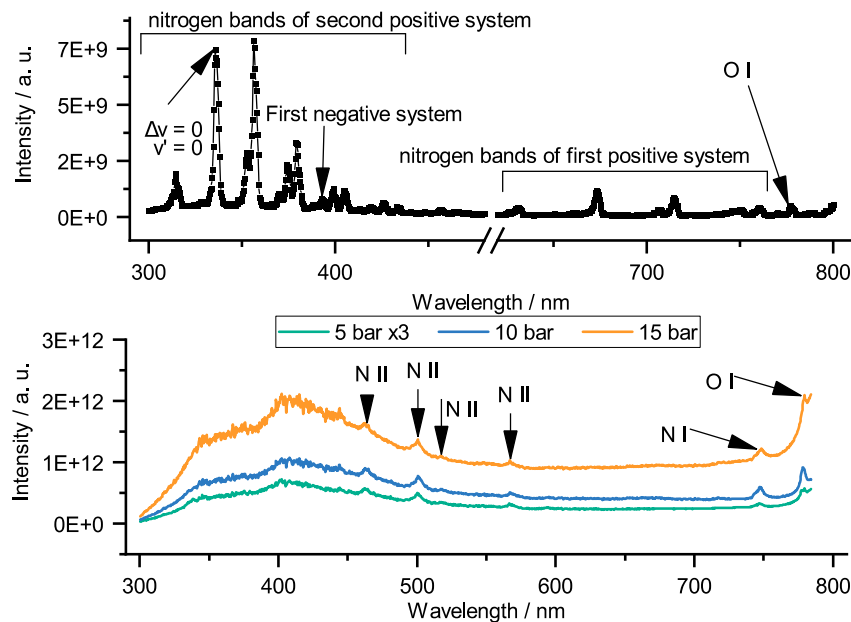


Fig. 5: Effect of the pressure on the measured breakdown voltage (U_{BD}), the static breakdown voltage (U_{Stat}) and their ratio on top, the initial current of the inductance on the left, and the duration of arc and glow discharge on the right.

3.2 Spectra of the Breakdown

At atmospheric pressure, the spectrum is shaped by the nitrogen bands of the first positive system (FPS) between 600 and 770 nm, the second positive system (SPS) between 300 and 430 nm, as well as the first negative system (FNS) with its transition at 391.4 nm, as shown in the upper graph of Fig. 6. In the at the right edge of the spectrum, the triple transition of the atomic oxygen at 777.2-777.5 nm is also visible. This shape of the spectrum is preserved up to a pressure of four bar, above which the spectrum suddenly changes to continuum radiation with intense atomic nitrogen radiation. Three examples of this continuum are shown in the bottom graph of Fig. 6. The change in the shape of the spectrum indicates a change of the physical mechanism of the breakdown. At low pressures, the breakdown appears to be initiated by the townsend mechanism, in which the main reason for the formation of a conductive channel is electron collisions. On the other hand, the continuum radiation appears to be a mixture of different physical mechanisms such as, photo-ionization, electron interaction (free-free) and recombination (electron-ion interaction, free-bound) [27–29]. These mechanisms occur in the process of the streamer formation described in chapter 1.2.1.



Influence of the Pressure on Spatial and Temporal Resolved Plasma Physical Parameters on a TCI-Ignition System

Fig. 6: Spectrum of the breakdown at atmospheric pressure (upper graph) and higher pressures (lower graph) at a temperature of 20 °C and synthetic air.

As the pressure increases, the electrical energy stored in the capacitances of the ignition system also increases, which is shown in the left graph of Fig. 7. For calculation of the energy, the capacitor C_{SP2} was used. The resulting energy with using this capacitance is in the range of 0.2 to 4 mJ. This energy range is slightly underestimated because it is assumed, that the energy is only supplied by this one capacitance. In reality, the other capacitances of the ignition system discharge slightly during this phase and therefore add some of their energy to the breakdown.

The right graph of Fig. 7 shows the intensity of the continuum radiation as a function of the pressure. Since the continuum appears above pressures of four bar, the graph starts at this pressure. At first, the intensity increases nearly linear with the pressure until eight bar. Afterwards it has a degressive tendency. However, in this pressure range, the supplied electrical energy increases almost linear, which means there is a gap between supplied energy and radiation yield. The energy from this difference can probably be found in dissociation processes or gas heating.

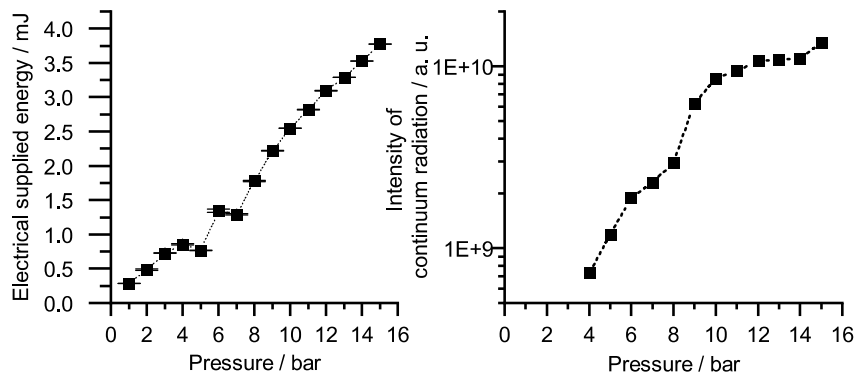


Fig. 7: Electric supplied energy (left) and intensity of the continuum radiation (right).

3.3 Spectra of the Arc Discharge

Fig. 8 shows the spectra of an arc discharge at atmospheric pressure in the upper and at higher pressures at the lower graph. All spectra are obtained from the near cathode region of the spark plug gap. At atmospheric pressure, the species of N_2 are overlaid by metal lines of iridium and rhodium from the center electrode material. Due to the low resolution used to obtain the spectrum, the different lines are not resolved and form a so-called pseudo-continuum, which is shown resolved in the small lower graph. With increasing pressure, the radiation from the nitrogen molecules is masked by the metal lines and can no longer be detected. The radiation of the metal lines is a direct result of the melting and evaporation of the electrode material due to the thermionic-field emission of the arc discharge.

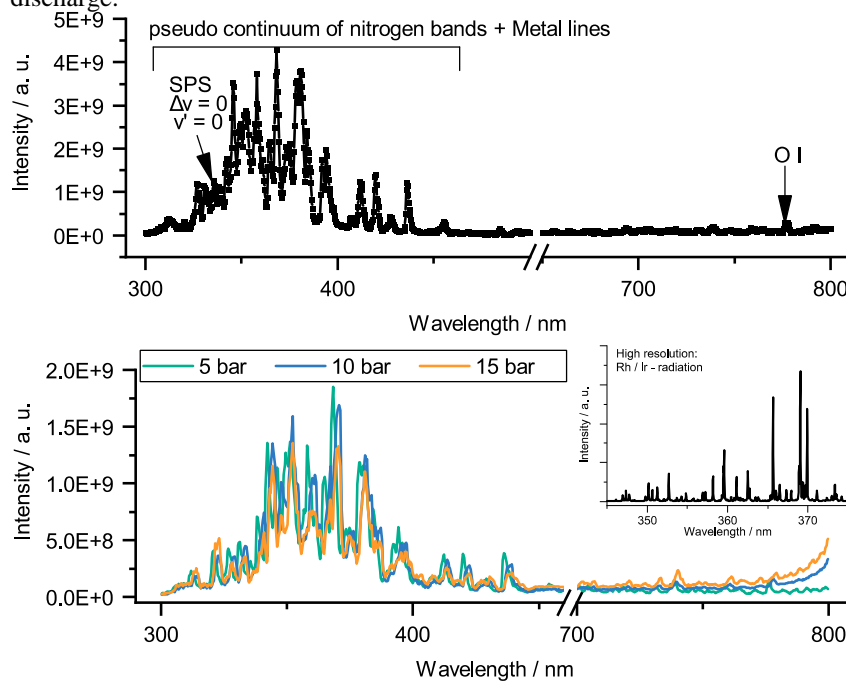


Fig. 8: Spectrum of the arc discharge at atmospheric pressure (upper graph) and higher pressures (lower graph) at a temperature of 20 °C and synthetic air. The small graph shows a high-resolution spectrum between 345 and 375 nm.

Influence of the Pressure on Spatial and Temporal Resolved Plasma Physical Parameters on a TCI-Ignition System

The intensity of the metal radiation is proportional to the particle density of the observed material, assuming a constant excitation temperature. The formulaic connection between the intensity ε_{ji} and the particle density n_0 is described by equation (3)

$$\varepsilon_{ji} = \frac{h * c_o}{4 * \pi * \lambda_{ji}} * A_{ji} * n_j \quad (3)$$

with the boltzmann distribution equation (4)

$$n_j = \frac{g_j}{U(T)} * n_0 * e^{-\frac{E_j}{k_B * T_{exc}}} \quad (4)$$

The equations contain the Planck constant h , the speed of light in vacuum c_o , the wavelength of the transition λ_{ji} , the transition probability A_{ji} , the occupation density of the particle n_j , the statistic weight g_j , state sum $U(T)$, the energy of the upper state E_j , the Boltzmann constant k_B and the excitation temperature T_{exc} .

Therefore, the intensity of a line is connected to the material evaporated by the cathode spot of the arc discharge. The more electrode material there is in the gas, the greater the probability that some of the released atoms will leave the electrode and thus wear it out.

The left graphic of Fig. 9 shows the supplied electrical energy, power and exposure time as a function of the pressure. Up to a pressure of three bar, the energy and power of the arc discharge increase. After that, both remain at a constant level until the pressure reaches nine bar, at which point they decrease again. This is explained by the reduction of the initial current, which makes it harder to reach the necessary current density for an arc discharge.

On the right graph of Fig. 9 the intensity of the $5d^76s(^5F)6p \rightarrow 5d^8(^3F)6s$ iridium transition in dependence of the pressure is shown. The intensity of this line is not mixed up with the intensity of the pseudo-continuum from Fig. 8. The rise of the intensity at a pressure of seven bar is obviously. Even with decrease of the electrical supplied power and energy, the intensity remains at a high level or is even increases with pressure. A reason for this behavior could be the contraction of the plasma channel and the cathode spot area due to the higher charge carrier particle density which can be achieved at these pressures. The decrease between 13 and 15 bar correlates with the decrease of supplied energy, power and the reduction of the initial current of the discharge.

Influence of the Pressure on Spatial and Temporal Resolved Plasma Physical Parameters on a TCI-Ignition System

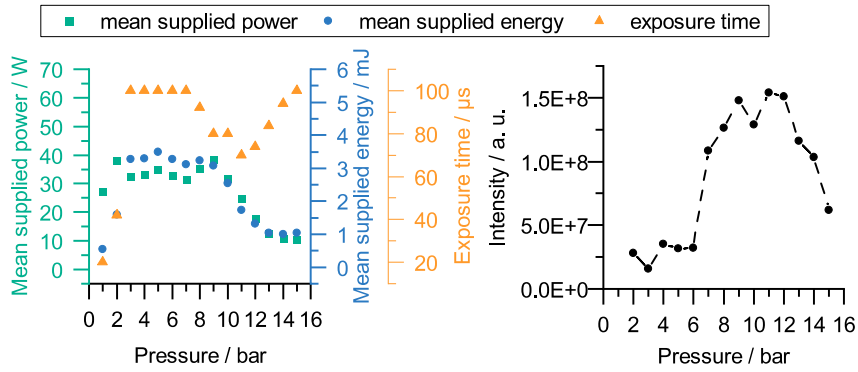


Fig. 9: Influence of the pressure on the supplied power, energy and exposure time (left), and the intensity of Ir-radiation.

3.4 Spectra of the Glow Discharge

The spectrum of the glow discharge has only minor changes with increasing pressure, as shown in Fig. 10. Like in the breakdown, the second positive system majorly shapes the spectrum. In the negative glow of this discharge, strong emissions of the FNS $\Delta v = 0$ are observed. In the remaining part of the plasma column this emission is not very bright. The strong presence of the FNS in the negative glow is a typical indicator for this area of the glow discharge, due to the high ionization processes.

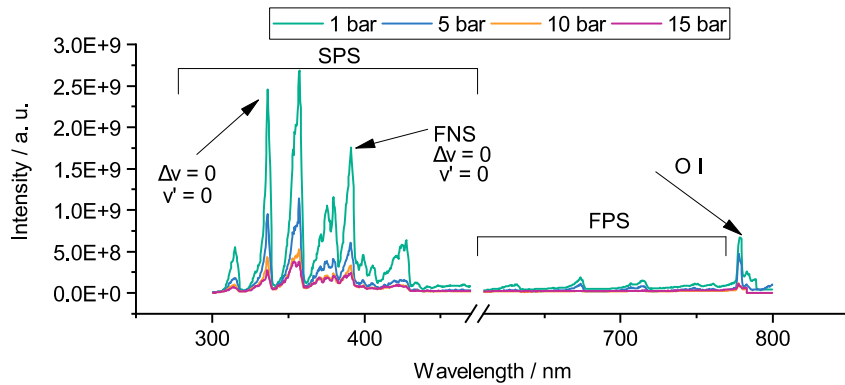


Fig. 10: Spectrum of the glow discharge in the negative glow at different pressures and a temperature of 20 °C with synthetic air.

Influence of the Pressure on Spatial and Temporal Resolved Plasma Physical Parameters on a TCI-Ignition System

In the left graph of Fig. 11, the electrical supplied power and energy are shown. With increasing pressure, both decrease slightly. At seven bar, the exposure time was doubled to sustain the signal-to-noise ratio of the measurements, so the supplied energy increases at this pressure.

The dependence of the intensity across the entire gap as a function of the pressure is shown in the right graph of Fig. 11. It shows a decreasing trend until a pressure of seven bar. From this point on, the intensity does not remain on a constant level. This constant level could be a remnant of the data acquisition process, in which measurements below a certain level were not recorded. Remarkable is the difference between one and two bar. At one bar, the discharge is significantly brighter and varies much less than at two bar. This can be explained by the spatial propagation in the radial direction of the discharge. At one bar, the discharge propagates the whole cathode, therefore its intensity remains very constant. With increasing pressure, the discharge contracts and cannot propagate the entire cathode anymore. Therefore, it is possible, that the discharge misses the optical path of the lens and the slit of the spectrograph. This results in lower intensities and the higher fluctuation of it.

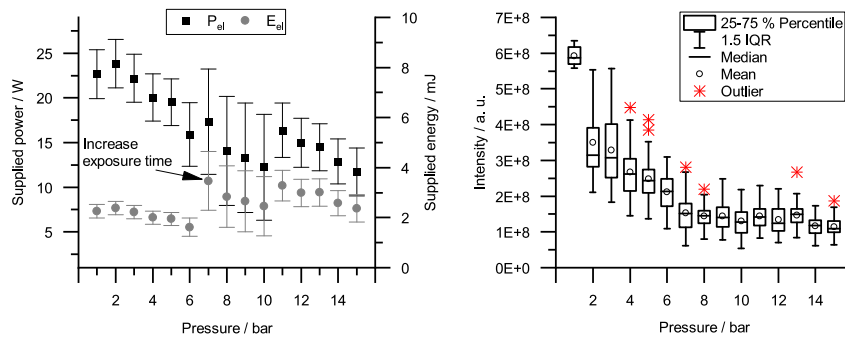


Fig. 11: Electrical supplied power and energy, and Intensity of the N_2 SPS $\Delta v = 0$ band as a function of gas pressure.

4 Discussion

The spectra of the three ignition phases differ significantly from each other. Therefore, it is necessary to obtain different methods of data acquisition to each phase and to apply different methods to determine plasma characteristics such as temperatures or particle densities.

The breakdown is the brightest phase of the ignition spark. Up to a pressure of three bar, N_2 band spectra can be observed, which can be used to determine rotational and vibrational temperature by comparing measured with simulated spectra. Above four bar, the continuum radiation could be used to determine particle densities and electron temperature. For these values, the absolute radiance of the plasma has to be obtained, which is not possible with the measurement setup used. Another approach is the determination of excitation temperature via the NII ions in the range of 500 nm using the line ratio method, which was performed, for example, by [30, 31]. In addition, the NII lines at 500 nm can be used to obtain the electron density due to stark broadening. This method is for example used in [32].

Due to the thermionic-field emission and the volatile oxides in the arc discharge, only metal lines could be observed. This makes it difficult to determine a temperature from the gas in this phase. However, the metal lines can be used to determine an excitation temperature of these metal lines by using the boltzmann-plot method. The prerequisite for this method is, that the metal lines used are carefully selected and the resolution has to be as high as possible to obtain accurate measurement results [33]. Nevertheless, the metal intensities can be used to estimate the intensity and erosion behavior of the observed arc discharge.

In the glow discharge, the N_2 bands of the second positive system and the first negative system are easily measurable. Therefore, they can be used to determine the rotational and vibrational temperature of this discharge. Moreover, by calculating the rate coefficients, the electron temperature can be determined by the line ratio method using the first negative system and the second positive system, as shown in [34]. The spatial area used to calculate these temperatures has to be chosen carefully because the temperatures depend strongly on the axial height of the discharge [9, 24, 25, 35].

5 Conclusion

In this work, we showed a measurement setup and methods for determining the influence of the pressure on the spectra of the ignition phases. The spectra showed significant influence from the pressure and the observed ignition phase. Also, the results show, that the ignition spark cannot be described by a single plasma-physical parameter. Rather, it is necessary to apply different methods to determine characteristic plasma-physical quantities of the phase. Furthermore, it was shown that the measurement setup used is suitable to estimate the intensity of arc discharge in terms of the release of electrode material into the gas. In the next steps, different calculation methods will be applied to determine the characteristic plasma parameters for each phase.

References

- [1] H. Albrecht, W. H. Bloss, W. Herden, R. Maly, B. Saggau, and E. Wagner, "New Aspects on Spark Ignition," in *SAE Technical Paper Series*, 1977, pp. 1–11.
- [2] H. Albrecht, R. Maly, W. H. Bloss, W. Herden, B. Saggau, and E. Wagner, "Neue Ergebnisse über die Entflammung durch den elektrischen Funken," *4th Statusseminar Kraftfahrzeug- und Straßenverkehrstechnik*, 1977, 1977.
- [3] H. Albrecht, R. Maly, B. Saggau, E. Wagner, and W. Herden, "Neue Erkenntnisse über elektrische Zündfunken und ihre Eignung zur Entflammung brennbarer Gemische," *Automobil-Industrie*, vol. 22, no. 4, pp. 45–50, 1977.
- [4] W. Herden, R. Maly, B. Saggau, and E. Wagner, "Neue Erkenntnisse über elektrische Zündfunken und ihre Eignung zur Entflammung brennbarer Gemische -2. Teil," *Automobil-Industrie*, vol. 23, no. 2, pp. 15–22, 1978.
- [5] R. Maly *et al.*, "Die drei Phasen einer elektrischen Zündung und ihre Auswirkungen auf die Entflammungseinleitung," *5th Statusseminar Kraftfahrzeuge und Straßenverkehr*, 1978, 1978.

Influence of the Pressure on Spatial and Temporal Resolved Plasma Physical Parameters on a TCI-Ignition System

- [6] R. Maly, "Spark Ignition: Its Physics and Effect on the Internal Combustion Engine," in *Fuel Economy: in Road Vehicles Powered by Spark Ignition Engines*, New York: Springer US, 1984, pp. 91–148.
- [7] R. Maly and M. Vogel, "Initiation and propagation of flame fronts in lean CH₄-air mixtures by the three modes of the ignition spark," *Symposium (International) on Combustion*, vol. 17, no. 1, pp. 821–831, 1979, doi: 10.1016/S0082-0784(79)80079-X.
- [8] R. R. Maly, "Die Zukunft der Funkenzündung," *MTZ - Motortechnische Zeitschrift*, vol. 59, no. 7, pp. XIX–XXIV, 1998, doi: 10.1007/BF03226465.
- [9] T. Michler, W. Kim, O. Toedter, T. Koch, and C. Bae, "Influence of the Electrical Parameters of the Ignition System on the Phases of Spark Ignition," in *Ignition Systems for Gasoline Engines: 4th International Conference, December 6-7, 2018, Berlin, Germany. Ed.: M. Günther*, 2018, pp. 222–238.
- [10] J. Rager, *Funkenerosion an Zündkerzenelektroden*. Aachen: Shaker, 2006.
- [11] J. S. E. Townsend, *Electrons in gases*: London : Hutchinson's scientific and technical publications, 1947. [Online]. Available: <http://lib.ugent.be/catalog/rug01:000701075>
- [12] J. S. E. Townsend, *Electricity in Gases*: Clarendon Press, 1915. [Online]. Available: <https://books.google.de/books?id=OQJaQAACA AJ>
- [13] J. S. E. Townsend and H. T. Tizard, "The Motion of Electrons in Gases," *Proceedings of the Royal Society A: Mathematical, Physical and Engineering Sciences*, vol. 88, no. 604, pp. 336–347, 1913, doi: 10.1098/rspa.1913.0034.
- [14] A. Küchler, *Hochspannungstechnik: Grundlagen, Technologie, Anwendungen*, 3rd ed.: Springer-Verlag, 2009.
- [15] J. M. Meek and J. D. Craggs, Eds., *Electrical breakdown of gases*. Oxford: Clarendon Press, 1953.
- [16] L. B. Loeb, *Basic processes of gaseous electronics*. Berkeley, Calif. [u.a.]: Univ. of California Pr, 1955.
- [17] H. Raether, *Electron avalanches and breakdown in gases*. London: Butterworths, 1964.
- [18] W. Ramberg, "Über den Mechanismus des elektrischen Lichtbogens," *Ann. Phys.*, vol. 404, no. 3, pp. 319–352, 1932, doi: 10.1002/andp.19324040305.

Influence of the Pressure on Spatial and Temporal Resolved Plasma Physical Parameters on a TCI-Ignition System

- [19] B. Jüttner, "Cathode spots of electric arcs," *J. Phys. D: Appl. Phys.*, vol. 34, no. 17, R103-R123, 2001. [Online]. Available: <http://stacks.iop.org/0022-3727/34/i=17/a=202>
- [20] A. Güntherschulze, "Zusammenhang zwischen Stromdichte und Kathodenfall der Glimmentladung bei Verwendung einer Schutzringkathode und Korrektur der Temperaturerhöhung des Gases," *Zeitschrift für Physik*, vol. 49, no. 5, pp. 358–379, 1928, doi: 10.1007/BF01337924.
- [21] A. Fridman and L. A. Kennedy, *Plasma Physics and Engineering, Second Edition*, 2nd ed. Hoboken: CRC Press, 2011.
- [22] J. P. Raizer, *Gas discharge physics*. Berlin: Springer, 1991.
- [23] A. Güntherschulze, "Die Abhängigkeit des normalen Kathodenfalles der Glimmentladung von der Gasdichte," *Zeitschrift für Physik*, vol. 49, no. 7, pp. 473–479, 1928, doi: 10.1007/BF01333631.
- [24] T. Michler, O. Toedter, and T. Koch, "Spatial and time resolved determination of the vibrational temperature in ignition sparks by variation of the dwell time," *SN Applied Sciences*, vol. 2, no. 7, p. 1311, 2020, doi: 10.1007/s42452-020-3104-6.
- [25] T. Michler, O. Toedter, and T. Koch, "Measurement of temporal and spatial resolved rotational temperature in ignition sparks at atmospheric pressure," *Automot. Engine Technol.*, vol. 5, 1-2, pp. 57–70, 2020, doi: 10.1007/s41104-020-00059-w.
- [26] K. B. Yahia, "Hybridmodellierung der Anfangsphase der Zündung einer Gasentladung," Dissertation, Universität Karlsruhe, Karlsruhe, 2002.
- [27] S. Park, W. Choe, H. Kim, and J. Y. Park, "Continuum emission-based electron diagnostics for atmospheric pressure plasmas and characteristics of nanosecond-pulsed argon plasma jets," *Plasma Sources Science and Technology*, vol. 24, no. 3, p. 34003, 2015, doi: 10.1088/0963-0252/24/3/034003.
- [28] S. Park, W. Choe, S. Youn Moon, and J. Park, "Electron density and temperature measurement by continuum radiation emitted from weakly ionized atmospheric pressure plasmas," *Appl. Phys. Lett.*, vol. 104, no. 8, 084103-1 - 084103-5, 2014, doi: 10.1063/1.4866804.
- [29] K. T. A. L. Burm, "Continuum radiation in a high pressure argon-mercury lamp," *Zeitschrift für Physik*, vol. 13, no. 3, pp. 387–394, 2004, doi: 10.1088/0963-0252/13/3/004.

Influence of the Pressure on Spatial and Temporal Resolved Plasma Physical Parameters on a TCI-Ignition System

- [30] N. Minesi, P. Mariotto, G.-D. Stancu, and C. O. Laux, "Ionization Mechanism in a Thermal Spark Discharge," in *AIAA Scitech 2021 Forum*, VIRTUAL EVENT, 01112021.
- [31] N. Minesi, S. Stepanyan, P. Mariotto, G. D. Stancu, and C. O. Laux, "Fully ionized nanosecond discharges in air: the thermal spark," *Plasma Sources Science and Technology*, vol. 29, no. 8, 2020, doi: 10.1088/1361-6595/ab94d3.
- [32] A. M. EL Sherbini, A. M. Aboufotouh, and C. G. Parigger, "Electron number density measurements using laser-induced breakdown spectroscopy of ionized nitrogen spectral lines," *Spectrochimica Acta Part B: Atomic Spectroscopy*, vol. 125, pp. 152–158, 2016, doi: 10.1016/j.sab.2016.10.003.
- [33] A. Mašláni, V. Sember, T. Stehrer, and H. Pauser, "Measurement of Temperature in the Steam Arcjet During Plasma Arc Cutting," *Plasma Chemistry and Plasma Processing*, vol. 33, no. 3, pp. 593–604, 2013, doi: 10.1007/s11090-013-9443-y.
- [34] A. Zerrouki, H. Motomura, Y. Ikeda, M. Jinno, and M. Yousfi, "Optical emission spectroscopy characterizations of micro-air plasma used for simulation of cell membrane poration," *Plasma Physics and Controlled Fusion*, vol. 58, no. 7, p. 75006, 2016, doi: 10.1088/0741-3335/58/7/075006.
- [35] D. Staack, B. Farouk, A. F. Gutsol, and A. Fridman, "Spatially Resolved Temperature Measurements of Atmospheric-Pressure Normal Glow Microplasmas in Air," *IEEE Trans. Plasma Sci.*, vol. 35, no. 5, pp. 1448–1455, 2007, doi: 10.1109/TPS.2007.904959.